ACS OMEGA

Article

Cite This: ACS Omega 2019, 4, 21260−21266

http://pubs.acs.org/journal/acsodf

Fabrication of a Highly Flexible and Affordable Transparent Electrode By Aligned U-Shaped Copper Nanowires Using a New Electrospinning Collector with Convenient Transferability

Mohammad Javad Nikzad,[†] Nima Mohamadbeigi,[†] Seyed Khatiboleslam Sadrnezhaad,*[,‡] and Seyed Mohammad Mahdavi[†,§]

[†]Institute for Nanoscience and Nanotechnology (INST), Sharif University of Technology, P.O. BOX 14588-89694, Tehran, Iran
[‡]Department of Materials Science and Engineering, Sharif University of Technology, P.O. BOX 11365-9466, Tehran, Iran
[§]Department of Physics, Sharif University of Technology, P.O. BOX 11365-9161, Tehran, Iran

ABSTRACT: By making aligned and suspended copper nanowires, a high performance, transferable, and flexible transparent electrode is reported. Indium tin oxide is often used in devices such as displays, solar cells, and touchscreens that require transparent and conductive plates. Because of problems such as brittleness, high cost, and environmental effects, this material is facing rivals, the most serious of which are metallic nanowire meshes, especially copper. We developed a simple technique which uses a U-shaped collector in the electrospinning process with three advantages including the enhancement of the figure of merit (which is related to the surface resistance R_s and the transmittance T) by about five times (about T = 90% and R_s = 5 Ω/□, respectively), solving the transfer problem of the nanowire metal mesh after production, and producing aligned metal nanowires for special applications. In this work, T and R_s of aligned copper nanowires were both measured and calculated, which are consistent with each other, and also, the mentioned results were compared with the work of others.

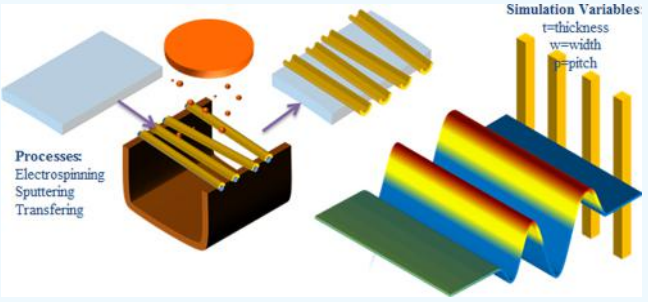

1. INTRODUCTION

The significant increase in demand from optoelectronic devices such as displays, solar cells, and touchscreens has stimulated the development of transparent conductive electrodes (TCEs) as an essential part of these devices. Given the growing the use of smartphones, tablets, laptops, liquid crystal displays, organic light-emitting diodes, and other optoelectronic apparatus, the global TCE market has reached $7.1 billion in 2018.[1,2] Today, indium tin oxide (ITO) is most commercially used to produce TCEs between various metal oxides.[2] The reasons for the popularity of ITO are low sheet resistance (R_s = 10−100 Ω/□) at high transparency (T > 85%), which led to the creation of a $ 5.1 billion market in 2017.[2,3] However, ITO suffers from several limitations, including its high cost, scarcity of indium, adverse environmental effects, high-temperature fabrication, and ionic diffusion into organic displays and brittleness, which makes it unsuitable for future mechanically flexible devices.[2,4−7] Thus, considering the fragility characteristics of ITO, alternative materials should be used to produce flexible transparent electrodes.[8]

Flexible TCEs have attracted particular attention in recent years to fabricate bendable or foldable displays, flexible solar cells, electronic papers, wearable devices, skin displays, and soft lightings.[2,9] Therefore, the development of flexible electrode technology is necessary to overcome the defects of ITO-based TCEs. Heretofore, researchers have introduced various materials such as oxide semiconductors, conductive polymers,[10−12] and nanostructure layers[3] for the production of these TCEs. Today, nanotechnology creates much hope for the development of the highly flexible TCEs with superb conductivity and transparency. Among the nanostructured transparent electrodes such as carbon nanotubes,[13−16] carbon nanobuds,[17−20] graphene,[21−28] hybrid structures,[16,17,23,29−33] and metal nanowire meshes,[34−39] the last one due to having suitable features such as high electrical conductivity, low-cost materials, and excellent mechanical properties can be considered as a promising candidate for the production of flexible TCEs.[1,40] However, extensive junction resistance due to the percolation of charges through junctions between different nanowires leads to drop the electrical conductivity of nanowire-based TCEs, which in some cases require thermal processes to reduce the electrical resistance of the junctions that may raise prices of the finished product.[41−43] Also, an appropriate volume of metal nanowires must be deposited to reach the percolation threshold for achieving high conductivity and maintain good transparency. Basically, in the multistep fabrication method, a metal mesh is constructed on the primary substrate and then transmitted to the final substrate,

Received: August 26, 2019
Accepted: November 26, 2019
Published: December 5, 2019

DOI: 10.1021/acsomega.9b02760
ACS Omega 2019, 4, 21260−21266

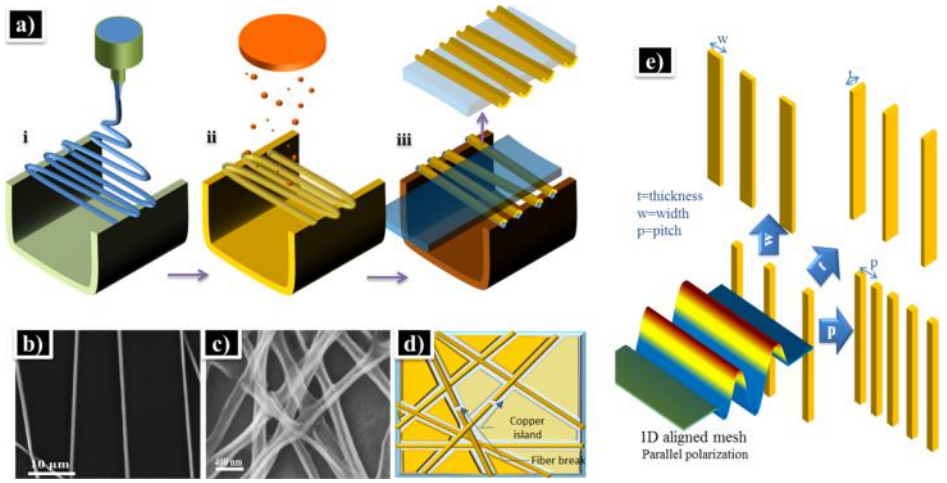

Figure 1. (a) Schematic of the aligned copper nanowires process for fabricating transparent electrodes. The polymer nanofiber template was first made by electrospinning and then coated with copper using the sputtering method. The coated wires were transferred onto a final substrate. (b) SEM image of obtained aligned wires with a new collector. (c) SEM image of the random copper nanowire mesh after removal of the polymer and turning upside down from closer view with the usual collector for comparison. Random U-shaped nanowires are recognizable. (d) Schematic problems in the usual collector. During the layer deposition process, the remainder component between wires leads to reduced transparency and efficiency. Also, during the transfer to another substrate, the wires would break. The suspended wires described in this work make the transfer very easy. (e) Definition of the optical 3D model with its directions and abbreviations. Pitch, thickness, and width of the nanowires in the mesh were considered to find which geometric structure is better. The shown waveform has parallel polarization with aligned wires.

which in turn causes the failure of some of the metal wires and reduces the efficiency. Also, during the sputtering process to metalize polymeric meshes, owing to the formation of separate islands on the substrate, which unlikely has an electrical junction with each other, the transparency reduces sharply. It eliminates the possibility of using the primary substrate in the final product.

Herein, using a particular collector in the electrospinning process, align and hovering polymeric wires were made as a template, and then, the copper metal was deposited on the produced template by a sputtering method. Finally, prepared nanowires were transmitted on the high flexible substrate to achieve the aligned U-shaped copper nanowires for creating roll-folding TCEs. Although copper has less electrical conductivity than silver and can be oxidized in air, because of its low cost and availability, it is still a better option than silver and gold, and the challenge of oxidizing it can be overcome with protective coatings.[44−46] The synthesis of these aligned U-shaped nanowires due to the decrease in the number of nanowires junction and the consequent reduction of their electrical resistance results in the production of highly flexible TCEs with remarkable properties. In this way, the challenges of nanowires transition on the substrate and unplugged metal islands were solved. Production of nanowires with this method is less costly than other methods such as lithography and solution-based and the only sputtering process in this way has a considerable cost. Today, the sputtering process is commercially used to produce low-emission glass and ITO transparent electrode that reduces its cost.

According to the high impact of the geometric properties of the metal mesh, such as the thickness of the U-shaped nanowires, the width of the wires and their density on the transparency and conductivity of the TCE, a set of experiments was designed and implemented to achieve the optimal geometric structure. Each of the experiments was studied in terms of transparency, electrical conductivity, geometric construction, and performance index. Besides, the wave optic simulations were performed, and after validation, they were used for studies and physical analyses of more samples.

2. METHODS

The fabrication of aligned metal nanowires was done in three main steps (Figure 1a), initially, (i) the fabrication of the polymeric template with electrospinning, (ii) metal sputtering on the template, and (iii) the transferring of nanowires. Polymer fibers were formed using the electrospinning instrument (ES1-Nanoazma Inc.) by selecting PVA (polyvinyl alcohol) and PEO (polyethylene oxide) polymers, making concentrations from 5 to 10% and a dc field 1.2 kV/cm. The tip-collector distance was adjusted at 12 cm with a flow rate of 2 mL/h. The nanofibers were collected on a U-shaped aluminum substrate with a length of 7 cm, a height of 2 cm, and a width of 1 cm to achieve aligned nanofibers.

To start electrospinning, a conductive U-shaped collector was used so that its electrostatic interaction with charged nanofibers aligns with collected fibers[47] (Figure 1b). The metal deposition process was carried out with a three-cathode sputtering machine (Nanostructured Coatings Inc.), a 99.99% copper target, a primary pressure of 10^{-5} Torr, a working pressure of 10^{-2} Torr, and an RF field of 120 W with a deposition rate of 15 nm/s.

In conventional methods, the wires are collected on a solid substrate randomly. Then, in the metal deposition process, the remainder islands on the substrate between wires lead to reduced transparency and efficiency (Figure 1d). Also, during the transfer to another substrate, the wires would break. However, fabricating of suspended wires in this work makes the transfer easy. By placing the substrate underneath and moving upward, the nanofibers are easily transferred to the substrate. Figure 1a step (iii) shows the copper nanowire mesh after removal of the polymer and turning it upside down.

To investigate the geometric structure of metal wires and determination of the optimal structure from the aspect of transparency and conductivity, the samples with more than 30

DOI: 10.1021/acsomega.9b02760
ACS Omega 2019, 4, 21260−21266

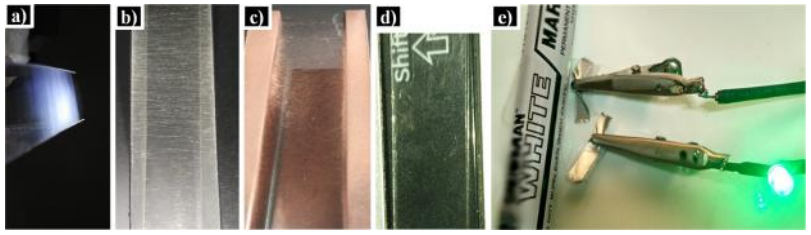

Figure 2. Aligned copper mesh in production steps (a) during electrospinning, (b) after electrospinning, and (c) after sputtering. (d) Transfer of wires to the solid substrate and (e) transfer of wires to the flexible layer and their use as a transparent electrode in the circuit.

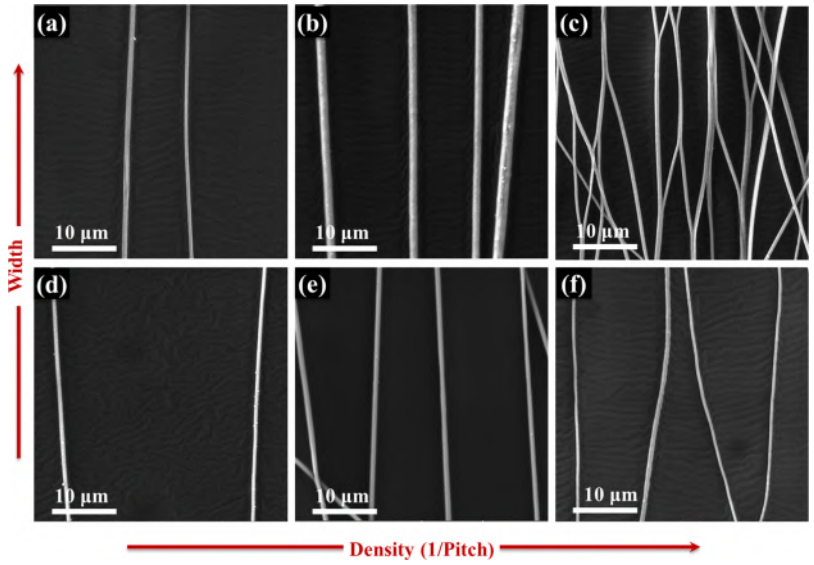

Figure 3. SEM images of six Cu aligned meshes at two width and three pitches in 5000× magnification. (a−c) are wider than (d−f) and the pitch increases from (a,d) to (b,e) and (c,f), respectively.

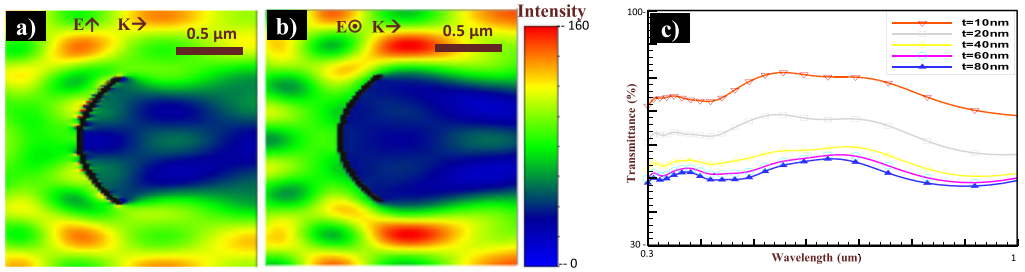

Figure 4. Optical simulation of aligned wires. (a) Intensity of light in the cross section of the nanowire with normal polarization to wire direction. (b) Same but in parallel polarization. (c) Transmittance of aligned copper wires with a pitch of 2 μm, a width of 1 μm, and a thickness of 10−80 nm at a wavelength of 0.3−1 μm.

geometries were produced in different widths, thicknesses, and pitches. Afterward, the surface resistance of the samples was measured using a 4-point-probe instrument (P100 Safir Soraya Inc.) and transparency of the specimens with an UV−vis instrument (Lambda950 PerkinElmer Inc.). Optical wave simulation performed based on Maxwell equations with the "Optiwave" software[48] by using the FDTD (finite-difference time-domain) method and the Drude−Lorentz material model. This model is used for obtaining optical coefficients that coincide with the experimental results of Rakić data[49] for copper. For the surfaces normal to the incident beam radiation, the perfectly matched layer boundary condition and for the side surfaces, the periodic boundary condition has been used. The incident wave is Gaussian type, the angle of incident is perpendicular to the metallic mesh, its power is 0.01 W, and its polarization angle is 0 and 90° to nanowire direction. Geometric simulation models were obtained by changing three parameters of thickness t, width w, and pitch p (Figure 1e).

3. RESULTS AND DISCUSSION

Figure 2 shows the aligned copper wires in production steps: electrospinning step (Figure 2a,b), after the sputtering step (Figure 2c), and after transferring it to the glass substrate (Figure 2d). Also, the wires are transferred to the flexible layer and are used as a transparent electrode in the circuit (Figure 2e).

The scanning electron microscopy (SEM) images of six samples of aligned metal wires are shown in two widths and three densities (1/pitch) in Figure 3a−f. In these images, the

DOI: 10.1021/acsomega.9b02760
ACS Omega 2019, 4, 21260−21266

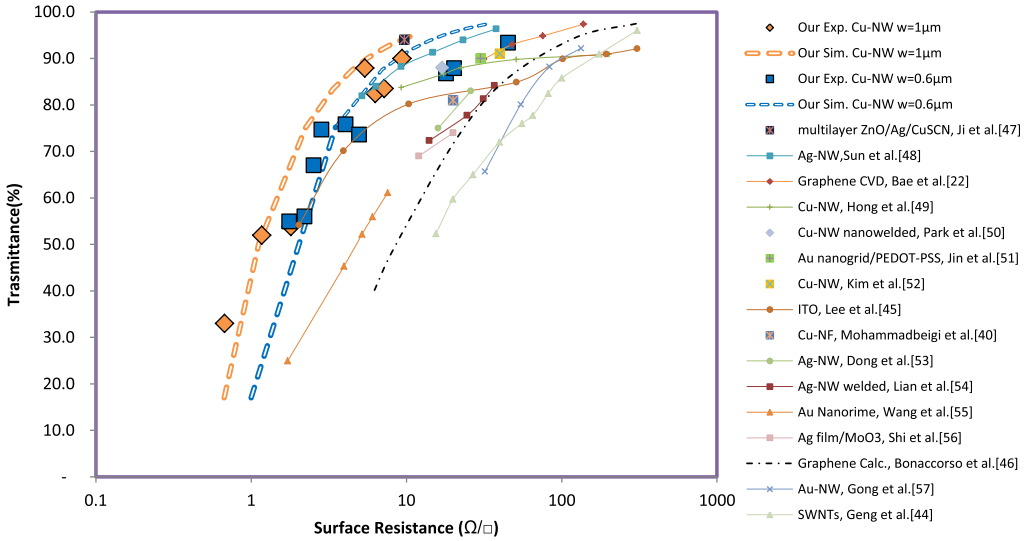

Figure 5. Transmittance at a wavelength of 550 nm and surface resistance of the aligned copper mesh for current experimental samples in two widths of 0.6 and 1 μm and their conformity with simulation results. Also, other works have been added for comparison.[50−59]

almost alignment and the preferred direction of the wires due to the electrostatic field between the nozzle and U-shaped collectors are observable. By increasing the density of wires and aggregation charge on the previous wire, the electric field around the collector changes and the alignment decreases.

After transferring metal nanowires to the substrate, surface resistance and transparency are measured with 4PP and UV−vis instruments. The results will be discussed later. Also, the optical simulation results for both E field and intensity are shown in Figure 4 when the linear polarized light is incident on a 1D mesh perpendicularly, and the polarization direction is normal (Figure 4a) or parallel to the wires (Figure 4b). These calculations are performed for different thicknesses at wavelengths from 0.3 to 1 μm to obtain the transmittance in each case (Figure 4c). The TC is also obtained from the simulation results. In the case of polarization parallel to nanowires, the aligned nanowire metal mesh absorbs more light because of current density along the wires, while in the case of normal polarization, the electrical field intensifies across the width of nanowires.

Also, the bending test was performed to test the flexibility of the transparent electrode. In this test, by increasing the bending radius to 7.5 mm, the electrical resistance increases by only 40%, indicating good flexibility of the transparent electrode.

The experimental and simulation results are plotted in terms of transmittance versus surface resistance Figure 5. The other works with ITO, graphene, and CNT have also been added for comparison. As it is seen, our experimental and calculated transparent electrodes show better optical and electrical properties than the best of the past: random silver mesh, graphene, and ITO.

Our experimental results are shown for two widths of 0.6 and 1 μm with blue squares and orange rhombuses, and their simulations with a dashed blue line and the solid orange line, respectively. Good conformity between experimental and simulated results is seen except in the upper part of the graph for narrower wires (higher surface resistance region). In this region, because the thickness of the metal in addition to the width of the wire is very thin, it is thought that the effect of growth defects such as impurities, crystalline defects, cracks, and islands is much higher than those thicker wires; therefore, the probability of cutting some of the electron pathways within the thin narrow wires becomes much higher than those in thick and wide wires. Consequently, experimental results in these regions show higher resistance than simulation prediction.

For a more precise comparison of the transparent electrodes produced under different conditions, we use the redefined figure of merit as follows

$$\mathrm{TC} = -1/(R_s \ln(T)) \quad (1)$$

where T is transparency, R_s is surface resistance, and TC is defined as the figure of merit of a transparent electrode. Using this relation, along with results of transparency measurement and surface resistance, the TC is represented versus metal thickness for different samples with a width of 0.6, 1, and 1.5 μm in Figure 6. The dotted lines are related to simulation and solid lines to experimental results. In cases where the width wires and the thickness of the metal layer are skinny, the

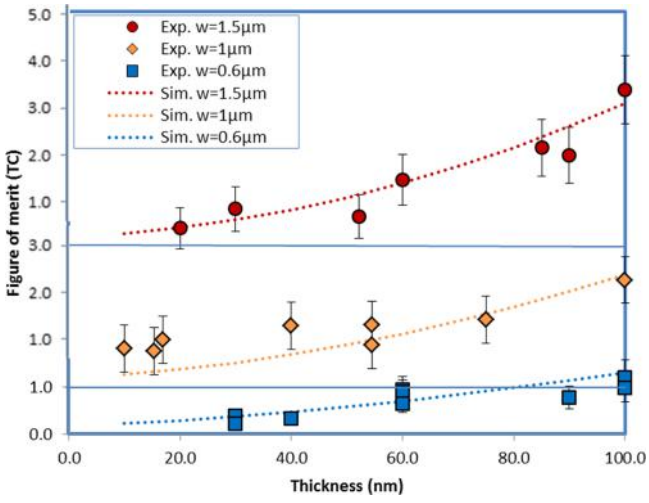

Figure 6. Figure of merit (TC) of the Cu aligned mesh in three widths vs wire thickness. Experimental results are shown by the markers and simulation results by dotted lines. The vertical axis is in multirange with three origins.

DOI: 10.1021/acsomega.9b02760
ACS Omega 2019, 4, 21260−21266

prediction of the simulation diagram differs from the experimental results of copper for the reason which already was said. In other cases, there is perfect conformity.

It can be seen that in all three charts, increasing the metal thickness improves the TC figure of merit. As it has already been mentioned, for low thicknesses, conductivity is more sensitive to crystalline defects; on the other hand, with increasing thickness, new pathways are created for restricted electron results in better conditions for a transparent flexible electrode. It is also observed that the chart of wider wires has a higher TC, while decreasing the width increases the electron scattering from boundaries and crystalline defects, which reduces the conductivity and TC.

The effect of mesh density (1/pitch) is negligible on the performance because if in the transparent electrode the density of the wires is increased, it means that the distance between the wires is decreased, while the width and thickness of each wire are fixed; consequently, both surface resistance and transparency are reduced and the figure of merit TC does not change.

4. CONCLUSIONS

By developing a simple technique which uses a U-shaped collector in the electrospinning process, we were able to make a flexible copper electrode with low surface resistance and high transmittance or a high figure of merit which is related to R_s and T. However, in prior methods, the random wires were produced on a solid substrate. In that solid substrate, the remaining components at the deposition step between the wires lead to reduce transparency and performance. Also, those wires are clinging to the solid substrate so that transferring them to the other substrate is accompanied by breaks and wrinkles. Therefore, transferring to various substrates by making suspended wires became easily accessible.

The results were also compared with the work of others. Because of the electrical and optical characteristics, it is hoped that our electrodes have a better performance.

AUTHOR INFORMATION

Corresponding Author

*E-mail: sadrnezh@sharif.edu.

ORCID

Mohammad Javad Nikzad: 0000-0002-6928-9151

Nima Mohamadbeigi: 0000-0003-4879-8907

Seyed Khatiboleslam Sadrnezhaad: 0000-0003-2631-5863

Notes

The authors declare no competing financial interest.

ACKNOWLEDGMENTS

The authors acknowledge the Sharif University of Technology and Iran National Science Foundation for their support of the research.

REFERENCES

(1) Shinde, M. A.; Mallikarjuna, K.; Noh, J.; Kim, H. Highly stable silver nanowires based bilayered flexible transparent conductive electrode. *Thin Solid Films* **2018**, *660*, 447−454.

(2) Zhang, C.; Nicolosi, V. Graphene and MXene-based transparent conductive electrodes and supercapacitors. *Energy Storage Mater.* **2019**, *16*, 102.

(3) Naghdi, S.; Rhee, K.; Hui, D.; Park, S. A review of conductive metal nanomaterials as conductive, transparent, and flexible coatings, thin films, and conductive fillers: Different deposition methods and applications. *Coatings* **2018**, *8*, 278.

(4) Kumar, A.; Zhou, C. The race to replace tin-doped indium oxide: which material will win? *ACS Nano* **2010**, *4*, 11−14.

(5) Schlatmann, A. R.; Floet, D. W.; Hilberer, A.; Garten, F.; Smulders, P. J. M.; Klapwijk, T. M.; Hadziioannou, G. Indium contamination from the indium−tin−oxide electrode in polymer light-emitting diodes. *Appl. Phys. Lett.* **1996**, *69*, 1764−1766.

(6) Chen, Z.; Cotterell, B.; Wang, W.; Guenther, E.; Chua, S.-J. A mechanical assessment of flexible optoelectronic devices. *Thin Solid Films* **2001**, *394*, 201−205.

(7) Kim, E.-H.; Yang, C.-W.; Park, J.-W. The crystallinity and mechanical properties of indium tin oxide coatings on polymer substrates. *J. Appl. Phys.* **2011**, *109*, 043511.

(8) Chen, X.; Guo, W.; Xie, L.; Zhuang, J.; Su, W.; Cui, Z. *43.2: Low Surface Roughness Transparent Conductive Electrode for QLED Applications, SID Symposium Digest of Technical Papers*; Wiley Online Library, 2018; pp 468−470.

(9) Ye, D.; Ding, Y.; Duan, Y.; Su, J.; Yin, Z.; Huang, Y. A. Large-Scale Direct-Writing of Aligned Nanofibers for Flexible Electronics. *Small* **2018**, *14*, 1703521.

(10) Li, R.; Parvez, K.; Hinkel, F.; Feng, X.; Müllen, K. Bioinspired wafer-scale production of highly stretchable carbon films for transparent conductive electrodes. *Angew. Chem., Int. Ed. Engl.* **2013**, *52*, 5535−5538.

(11) Zhang, X.; Wu, J.; Wang, J.; Zhang, J.; Yang, Q.; Fu, Y.; Xie, Z. Highly conductive PEDOT: PSS transparent electrode prepared by a post-spin-rinsing method for efficient ITO-free polymer solar cells. *Sol. Energy Mater. Sol. Cells* **2016**, *144*, 143−149.

(12) Yang, Y.; Heeger, A. J. Polyaniline as a transparent electrode for polymer light-emitting diodes: Lower operating voltage and higher efficiency. *Appl. Phys. Lett.* **1994**, *64*, 1245−1247.

(13) Kaskela, A.; Nasibulin, A. G.; Timmermans, M. Y.; Aitchison, B.; Papadimitratos, A.; Tian, Y.; Zhu, Z.; Jiang, H.; Brown, D. P.; Zakhidov, A.; Kauppinen, E. I. Aerosol-synthesized SWCNT networks with tunable conductivity and transparency by a dry transfer technique. *Nano Lett.* **2010**, *10*, 4349−4355.

(14) Facchetti, A.; Marks, T. J. *Transparent electronics*; Wiley Online Library: United Kingdom, 2010; pp 185−211.

(15) Pasquier, A. D.; Unalan, H. E.; Kanwal, A.; Miller, S.; Chhowalla, M. Conducting and transparent single-wall carbon nanotube electrodes for polymer-fullerene solar cells. *Appl. Phys. Lett.* **2005**, *87*, 203511.

(16) Virkar, A. Highly Conductivity and Transparent Carbon-Nanotube and Organic Semiconductor Hybrid Films: Exploiting Organic Semiconductor Energy Levels and Growth Mode. *Investigating the Nucleation, Growth, and Energy Levels of Organic Semiconductors for High Performance Plastic Electronics*; Springer: New York, 2012; pp 115−128.

(17) Nasibulin, A. G.; Pikhitsa, P. V.; Jiang, H.; Brown, D. P.; Krasheninnikov, A. V.; Anisimov, A. S.; Queipo, P.; Moisala, A.; Gonzalez, D.; Lientschnig, G.; Hassanien, A.; Shandakov, S. D.; Lolli, G.; Resasco, D. E.; Choi, M.; Tománek, D.; Kauppinen, E. I. A novel hybrid carbon material. *Nat. Nanotechnol.* **2007**, *2*, 156−161.

(18) Nasibulin, A. G.; Anisimov, A. S.; Pikhitsa, P. V.; Jiang, H.; Brown, D. P.; Choi, M.; Kauppinen, E. I. Investigations of NanoBud formation. *Chem. Phys. Lett.* **2007**, *446*, 109−114.

(19) Nicholls, R. J.; Britton, J.; Meysami, S. S.; Koós, A. A.; Grobert, N. In situ engineering of NanoBud geometries. *Chem. Commun.* **2013**, *49*, 10956−10958.

(20) Zhao, P.; Wang, P. J.; Zhang, Z.; Ren, M. J.; Liu, D. S. First-principles study of the electronic transport properties of the carbon nanobuds. *Phys. B* **2010**, *405*, 2097−2101.

(21) Khrapach, I.; Withers, F.; Bointon, T. H.; Polyushkin, D. K.; Barnes, W. L.; Russo, S.; Craciun, M. F. Novel Highly Conductive and Transparent Graphene-Based Conductors. *Adv. Mater.* **2012**, *24*, 2844−2849.

(22) Bae, S.; Kim, H.; Lee, Y.; Xu, X.; Park, J.-S.; Zheng, Y.; Balakrishnan, J.; Lei, T.; Ri Kim, H.; Song, Y. I.; Kim, Y.-J.; Kim, K. S.;

DOI: 10.1021/acsomega.9b02760
ACS Omega 2019, 4, 21260−21266

Özyilmaz, B.; Ahn, J.-H.; Hong, B. H.; Iijima, S. Roll-to-roll production of 30-inch graphene films for transparent electrodes. *Nat. Nanotechnol.* **2010**, *5*, 574−578.
(23) George, T.; Kholmanov, I. N.; Kim, T.; Domingues, S. H.; Kim, J.-Y.; Tan, C.; Magnuson, C. W.; Li, H.; Piner, R.; Ruoff, R. S.; Islam, M. S.; Dutta, A. K. *Graphene-Carbon Nanotube Hybrid Transparent Conductive Films*, 2013; Vol. *8725*, p 87251V.
(24) Nekahi, A.; Marashi, P. H.; Haghshenas, D. Transparent conductive thin film of ultra large reduced graphene oxide monolayers. *Appl. Surf. Sci.* **2014**, *295*, 59.
(25) Kim, K. S.; Zhao, Y.; Jang, H.; Lee, S. Y.; Kim, J. M.; Kim, K. S.; Ahn, J.-H.; Kim, P.; Choi, J.-Y.; Hong, B. H. Large-scale pattern growth of graphene films for stretchable transparent electrodes. *Nature* **2009**, *457*, 706−710.
(26) Gomez De Arco, L.; Zhang, Y.; Schlenker, C. W.; Ryu, K.; Thompson, M. E.; Zhou, C. Continuous, highly flexible, and transparent graphene films by chemical vapor deposition for organic photovoltaics. *ACS Nano* **2010**, *4*, 2865−2873.
(27) Jo, G.; Choe, M.; Cho, C.-Y.; Kim, J. H.; Park, W.; Lee, S.; Hong, W.-K.; Kim, T.-W.; Park, S.-J.; Hong, B. H.; Kahng, Y. H.; Lee, T. Large-scale patterned multi-layer graphene films as transparent conducting electrodes for GaN light-emitting diodes. *Nanotechnology* **2010**, *21*, 175201.
(28) Ahmad, R.; Shamsudin, M. S.; Sahdan, M. Z.; Rusop, M.; Sanip, S. M. Green and Economic Transparent Conductive Graphene Electrode for Organic Solar Cell: A Short Review. *Adv. Mater. Res.* **2013**, *832*, 316−321.
(29) Tung, V. C.; Chen, L.-M.; Allen, M. J.; Wassei, J. K.; Nelson, K.; Kaner, R. B.; Yang, Y. Low-temperature solution processing of graphene− carbon nanotube hybrid materials for high-performance transparent conductors. *Nano Lett.* **2009**, *9*, 1949−1955.
(30) Domingues, S. H.; Kholmanov, I. N.; Kim, T.; Kim, J.; Tan, C.; Chou, H.; Alieva, Z. A.; Piner, R.; Zarbin, A. J. G.; Ruoff, R. S. Reduction of graphene oxide films on Al foil for hybrid transparent conductive film applications. *Carbon* **2013**, *63*, 454−459.
(31) Lee, M.-S.; Lee, K.; Kim, S.-Y.; Lee, H.; Park, J.; Choi, K.-H.; Kim, H.-K.; Kim, D.-G.; Lee, D.-Y.; Nam, S.; Park, J.-U. High-Performance, Transparent, and Stretchable Electrodes Using Graphene−Metal Nanowire Hybrid Structures. *Nano Lett.* **2013**, *13*, 2814−2821.
(32) Shervedani, R. K.; Amini, A. Novel Graphene-Gold Hybrid Nanostructures Constructed via Sulfur Modified Graphene: Preparation and Characterization by Surface and Electrochemical Techniques. *Electrochim. Acta* **2014**, *121*, 376.
(33) Zou, J.; Yip, H.-L.; Hau, S. K.; Jen, A. K.-Y. Metal grid/conducting polymer hybrid transparent electrode for inverted polymer solar cells. *Appl. Phys. Lett.* **2010**, *96*, 203301.
(34) Gong, S.; Zhao, Y.; Yap, L. W.; Shi, Q.; Wang, Y.; Bay, J. A. P. B.; Lai, D. T. H.; Uddin, H.; Cheng, W. Fabrication of Highly Transparent and Flexible NanoMesh Electrode via Self-assembly of Ultrathin Gold Nanowires. *Adv. Electron. Mater.* **2016**, *2*, 1600121.
(35) Wu, H.; Kong, D.; Ruan, Z.; Hsu, P.-C.; Wang, S.; Yu, Z.; Carney, T. J.; Hu, L.; Fan, S.; Cui, Y. A transparent electrode based on a metal nanotrough network. *Nat. Nanotechnol.* **2013**, *8*, 421−425.
(36) Han, B.; Pei, K.; Huang, Y.; Zhang, X.; Rong, Q.; Lin, Q.; Guo, Y.; Sun, T.; Guo, C.; Carnahan, D.; Giersig, M.; Wang, Y.; Gao, J.; Ren, Z.; Kempa, K. Uniform Self-Forming Metallic Network as a High-Performance Transparent Conductive Electrode. *Adv. Mater.* **2013**, *26*, 873−877.
(37) Guo, H.; Lin, N.; Chen, Y.; Wang, Z.; Xie, Q.; Zheng, T.; Gao, N.; Li, S.; Kang, J.; Cai, D.; Peng, D. L. Copper nanowires as fully transparent conductive electrodes. *Sci. Rep.* **2013**, *3*, 2323.
(38) Kang, M.-G.; Guo, L. J. Nanoimprinted Semitransparent Metal Electrodes and Their Application in Organic Light-Emitting Diodes. *Adv. Mater.* **2007**, *19*, 1391−1396.
(39) Ricciardulli, A. G.; Yang, S.; Wetzelaer, G.-J. A. H.; Feng, X.; Blom, P. W. M. Hybrid Silver Nanowire and Graphene-Based Solution-Processed Transparent Electrode for Organic Optoelectronics. *Adv. Funct. Mater.* **2018**, *28*, 1706010.
(40) Celle, C.; Cabos, A.; Fontecave, T.; Laguitton, B.; Benayad, A.; Guettaz, L.; Pélissier, N.; Nguyen, V. H.; Bellet, D.; Muñoz-Rojas, D.; Simonato, J.-P. Oxidation of copper nanowire based transparent electrodes in ambient conditions and their stabilization by encapsulation: Application to transparent film heaters. *Nanotechnology* **2018**, *29*, 085701.
(41) Park, J. H.; Han, S.; Kim, D.; You, B. K.; Joe, D. J.; Hong, S.; Seo, J.; Kwon, J.; Jeong, C. K.; Park, H.-J.; Kim, T.-S.; Ko, S. H.; Lee, K. J. Plasmonic-Tuned Flash Cu Nanowelding with Ultrafast Photochemical-Reducing and Interlocking on Flexible Plastics. *Adv. Funct. Mater.* **2017**, *27*, 1701138.
(42) Mohamadbeigi, N.; Angizi, S.; Sadrnezhaad, S. K.; Nikzad, M. J. Improving the multi-step fabrication approach of copper nanofiber networks based transparent electrode for achieving superb conductivity and transparency. *Mater. Res. Express* **2019**, *6*, 095098.
(43) Che, B.; Zhou, D.; Li, H.; He, C.; Liu, E.; Lu, X. A highly bendable transparent electrode for organic electrochromic devices. *Org. Electron.* **2019**, *66*, 86−93.
(44) Kim, D.; Kwon, J.; Jung, J.; Kim, K.; Lee, H.; Yeo, J.; Hong, S.; Han, S.; Ko, S. H. A Transparent and Flexible Capacitive-Force Touch Pad from High-Aspect-Ratio Copper Nanowires with Enhanced Oxidation Resistance for Applications in Wearable Electronics. *Small Methods* **2018**, *2*, 1800077.
(45) Hong, I.; Roh, Y.; Koh, J. S.; Na, S.; Kim, T.; Lee, E.; An, H.; Kwon, J.; Yeo, J.; Hong, S.; Lee, K. T.; Kang, D.; Ko, S. H.; Han, S. Semipermanent Copper Nanowire Network with an Oxidation-Proof Encapsulation Layer. *Adv. Mater. Technol.* **2019**, *4*, 1800422.
(46) Hong, I.; Lee, S.; Kim, D.; Cho, H.; Roh, Y.; An, H.; Hong, S.; Ko, S. H.; Han, S. Study on the oxidation of copper nanowire network electrodes for skin mountable flexible, stretchable and wearable electronics applications. *Nanotechnology* **2018**, *30*, 074001.
(47) Li, D.; Wang, Y.; Xia, Y. Electrospinning of polymeric and ceramic nanofibers as uniaxially aligned arrays. *Nano Lett.* **2003**, *3*, 1167−1171.
(48) OptiWave Software, OptiFDTD Version 12.0. https://optiwave.com/resources/academia/free-fdtd-download/, January 2013.
(49) Rakić, A. D.; Djurišić, A. B.; Elazar, J. M.; Majewski, M. L. Optical properties of metallic films for vertical-cavity optoelectronic devices. *Appl. Opt.* **1998**, *37*, 5271−5283.
(50) Ji, Y.; Yang, J.; Luo, W.; Tang, L.; Bai, X.; Leng, C.; Ma, C.; Wei, X.; Wang, J.; Shen, J.; Lu, S.; Sun, K.; Shi, H. Ultraflexible and High-Performance Multilayer Transparent Electrode Based on ZnO/Ag/CuSCN. *ACS Appl. Mater. Interfaces* **2018**, *10*, 9571−9578.
(51) Sun, B.; Long, Y.-Z.; Chen, Z.-J.; Liu, S.-L.; Zhang, H.-D.; Zhang, J.-C.; Han, W.-P. Recent advances in flexible and stretchable electronic devices via electrospinning. *J. Mater. Chem. C* **2014**, *2*, 1209.
(52) Jin, S. W.; Lee, Y. H.; Yeom, K. M.; Yun, J.; Park, H.; Jeong, Y. R.; Hong, S. Y.; Lee, G.; Oh, S. Y.; Lee, J. H.; Noh, J. H.; Ha, J. S. Highly Durable and Flexible Transparent Electrode for Flexible Optoelectronic Applications. *ACS Appl. Mater. Interfaces* **2018**, *10*, 30706−30715.
(53) Lee, J.-Y.; Connor, S. T.; Cui, Y.; Peumans, P. Solution-processed metal nanowire mesh transparent electrodes. *Nano Lett.* **2008**, *8*, 689−692.
(54) Dong, J.; Goldthorpe, I. A. Exploiting both optical and electrical anisotropy in nanowire electrodes for higher transparency. *Nanotechnology* **2018**, *29*, 045705.
(55) Lian, L.; Xi, X.; Dong, D.; He, G. Highly conductive silver nanowire transparent electrode by selective welding for organic light emitting diode. *Org. Electron.* **2018**, *60*, 9−15.
(56) Wang, Y.; Gong, S.; Dong, D.; Zhao, Y.; Yap, L. W.; Shi, Q.; An, T.; Ling, Y.; Simon, G. P.; Cheng, W. Self-assembled gold nanorime mesh conductors for invisible stretchable supercapacitors. *Nanoscale* **2018**, *10*, 15948−15955.
(57) Shi, L.; Cui, Y.; Gao, Y.; Wang, W.; Zhang, Y.; Zhu, F.; Hao, Y. High Performance Ultrathin MoO(3)/Ag Transparent Electrode and

DOI: 10.1021/acsomega.9b02760
ACS Omega 2019, 4, 21260−21266

Its Application in Semitransparent Organic Solar Cells. *Nanomaterials* **2018**, *8*, 473.
(58) Bonaccorso, F.; Sun, Z.; Hasan, T.; Ferrari, A. C. Graphene photonics and optoelectronics. *Nat. Photonics* **2010**, *4*, 611−622.
(59) Geng, H.-Z.; Kim, K. K.; So, K. P.; Lee, Y. S.; Chang, Y.; Lee, Y. H. Effect of acid treatment on carbon nanotube-based flexible transparent conducting films. *J. Am. Chem. Soc.* **2007**, *129*, 7758−7759.

DOI: 10.1021/acsomega.9b02760
ACS Omega 2019, 4, 21260−21266